

An X-ray study of non-zero nickel moment in a ferromagnetic shape-memory alloy

Zahirul Islam^{a,*}, D. Haskel^a, J.C. Lang^a, G. Srajer^a, Y. Lee^b, B.N. Harmon^b, A.I. Goldman^b,
D.L. Schlagel^c, T.A. Lograsso^c

^aAdvanced Photon Source, Argonne National Laboratory, 9700 S. Cass Avenue, Argonne, IL 60439, USA

^bAmes Laboratory, Department of Physics and Astronomy, Iowa State University, Ames, IA 50011, USA

^cAmes Laboratory, Materials Science and Engineering Physics, Iowa State University, Ames, IA 50011, USA

Received 12 August 2005; received in revised form 12 October 2005

Available online 1 December 2005

Abstract

The existence of a magnetic moment at the nickel sites in ferromagnetic shape-memory alloys (FSMA) has long been speculated. Using a state-of-the-art X-ray magnetic circular dichroism (XMCD) technique we found that Ni 3d moments indeed exist in Ni–Mn–Ga-based FSMA. Band-structure calculations were used to simulate the XMCD spectra and estimate this moment to be $\sim 0.33 \mu_B$. Such a Ni moment plays a critical role in the dispersions of non-collinear spin structures, which determine the finite-temperature magnetic properties.

© 2005 Elsevier B.V. All rights reserved.

Keywords: Ferromagnetic shape-memory alloys; Martensitic transformation; X-ray magnetic circular dichroism; XMCD; Ni₂MnGa

1. Introduction

Within the large class of Heusler alloys [1] Ni₂MnGa is the first and most widely studied ferromagnet ($T_C \sim 350$ K) that shows shape-memory effects and magnetic field-induced large strains [2,3]. Magnetic properties of these ferromagnetic shape-memory alloys (FSMA) are primarily due to the ordering of the manganese (Mn) moments according to neutron-diffraction measurements [4]. A recent first-principles work, however, discussed the possibility of magnons in these materials involving nickel (Ni) moments [5]. Magnons can be treated as non-collinear spin structures of Mn and Ni moments (“frozen magnons”) to calculate finite-temperature properties including the paramagnetic to ferromagnetic transition, or Curie, temperature (T_C) [6]. It was shown that despite the smallness of the 3d moment at the Ni site it plays a critical role in the energetics of the frozen magnons [5]. Indeed, it is known that excess nickel in Ni–Mn–Ga FSMA decreases T_C

indicating the significance of Ni in their magnetic properties. Band-structure calculations on a group of related compounds reported that, while the minority-spin 3d states are excluded from the Mn sites (pushed above the Fermi energy, E_F), the Mn 3d majority-spin band hybridizes with Ni 3d band and results in a total moment with contributions on both sites [7]. An upper limit of $\sim 0.3 \mu_B$ was placed for the conjectured Ni moment from neutron measurements [4]. Recently, using numerical methods on polarized neutron diffraction data, Brown et al. showed not only the presence of magnetic moment on the nickel site but also a redistribution of that moment on going through the martensitic transformation (MT) [8]. Although their findings are model sensitive and differ from theoretical expectations [9] their work provide strong evidence for significant role played by Ni moments in the phase transition. Our primary objective is to show unambiguously the existence of a non-zero nickel moment in a Ni–Mn–Ga FSMA using model-independent and element-specific X-ray magnetic circular dichroism (XMCD) techniques.

Ni–Mn–Ga-based FSMA undergoes a MT near room temperature from a high-symmetry cubic phase (austenite)

*Corresponding author. Tel.: +1 630 252 9252; fax: +1 630 252 7392.

E-mail address: zahir@aps.anl.gov (Z. Islam).

into a lower-symmetry structure (e.g. tetragonal and/or orthorhombic) while remaining ferromagnetic throughout. What is remarkable, however, is the tunability of the MT and ferromagnetic transitions relative to each other by changing the stoichiometry from the ideal 2:1:1 composition. In addition to decreasing T_c excess nickel changes the MT temperature dramatically (60–70%) [10–12] in non-stoichiometric compounds. Such large changes brought about by Ni substitution can be qualitatively understood from the generalized electronic susceptibility calculations [13] which found that the lattice (phonon) softening [14,15] and MT in the ferromagnetic phase are due to Fermi-surface nesting involving the Mn and Ni 3d states, respectively. Furthermore, there are experimental indications of band Jahn–Teller effects critically involving Ni 3d electrons in the MT [8].

In this work, our focus is to study the element-specific magnetic properties of Ni in both the martensitic and austenitic phases in a non-stoichiometric (see below) Ni–Mn–Ga sample. At this composition there is an anomaly below the MT temperature (see below) and a very large field-induced strain ($\sim 5.7\%$) [3] has been reported. We used an XMCD technique at the K edge (8.333 keV) of Ni, which is ideal for this purpose. The K-edge dichroism measures the spin-dependent absorption due to $1s \rightarrow 4p$ transition into unoccupied bands above the E_F . Since there is no spin–orbit (SO) coupling in the 1s core state, SO splitting of the final 4p states is required for the K-edge dichroism signal. The presence of an XMCD effect, however, directly signifies the presence of a moment at the Ni site. Although this is an indirect probe of the 3d moments in contrast to the soft X-ray L-edge dichroism of transition metals, K-edge X-rays have much greater penetration depths. As such they are unaffected by surface effects and provide an excellent bulk sensitivity even near the absorption edge. Such a sensitivity is desirable in the study of intrinsic properties of these non-stoichiometric ternary compounds, where the presence of possible extraneous phases in minute quantities may give rise to spurious results. We observed significant XMCD effects ($\sim 0.3\%$) at the Ni K-edge in both martensitic and austenitic phases unambiguously showing the presence of a Ni 3d moment. Band-structure calculations accounting for the experimental XMCD spectra yielded a moment value of $\sim 0.33 \mu_B$.

The paper is organized as follows: experimental details and relevant sample information are given in the second section. In Section 3 the experimental evidence of Ni

moment is presented followed by band calculations to understand the XMCD spectra in Ni–Mn–Ga compared to that in elemental Ni. Next, XMCD spectra in martensitic and austenitic phases were compared. A brief summary of the work is presented in the last section.

2. Experimental details

Polycrystalline samples were prepared by arc melting an appropriate mixture of high-purity Ni, Mn, and Ga under an Ar atmosphere. The arc-melted ingots were pulverized and particles of different sizes were selected using appropriate meshes. Using SEM/EDS, the sample composition was determined to be $\text{Ni}_{48\pm 1}\text{Mn}_{30\pm 1}\text{Ga}_{22\pm 1}$. Structural and magnetic transition temperatures (Table 1) were measured on the powder using a differential scanning calorimetry (DSC) technique on both heating and cooling the sample. In addition to the ferromagnetic transition and MT, a weak transition is observed at ~ 285 K just below the MT.

For the XMCD measurements, polycrystalline samples (particle size $\sim 10 \mu\text{m}$) were mixed with a non-magnetic resin and cast into a thin disk that was mounted at the end of a He-flow cryostat and placed inside a horizontal field superconducting magnet. The XMCD measurements were carried out on the 4ID-D beamline at the Advanced Photon Source. This beamline is equipped with an in-line Bragg transmission-type phase retarder to convert linearly polarized monochromatic X-rays into circularly polarized X-rays of either helicity [16]. Two ion chambers, one before and one after the sample, were used in order to measure the X-ray absorption as a function of energy for each polarization state of the incoming X-rays. In order to increase the sensitivity to small moments and to eliminate systematic errors, we employed a lock-in technique [17]. In this technique the phase retarder was oscillated with a known frequency to generate X-rays of opposite helicities, and the modulation of the X-ray absorption coefficient at the oscillating frequency was detected.

We also collected powder-diffraction patterns on the same sample in order to identify the crystallographic phases involved in the MT. These data were collected with an incident beam energy of 8.3 keV (just below the Ni K-edge). A Ge(1 1 1) analyzer crystal was placed before a scintillator detector to suppress background and improve resolution. The sample temperature was varied, in this case, using a closed-cycle He refrigerator mounted on a Huber goniometer. The data were collected in the transmission

Table 1
Transition Temperatures (in Kelvin) from DSC

Martensitic				Ferromagnetic	
A_s	A_f	M_s	M_f	T_c (cooling)	T_c (heating)
310.2	347.1	336.4	309	367.9	369.9

A_s : Austenite start, M_f : Martensite finish, etc. T_c : Curie temperature.

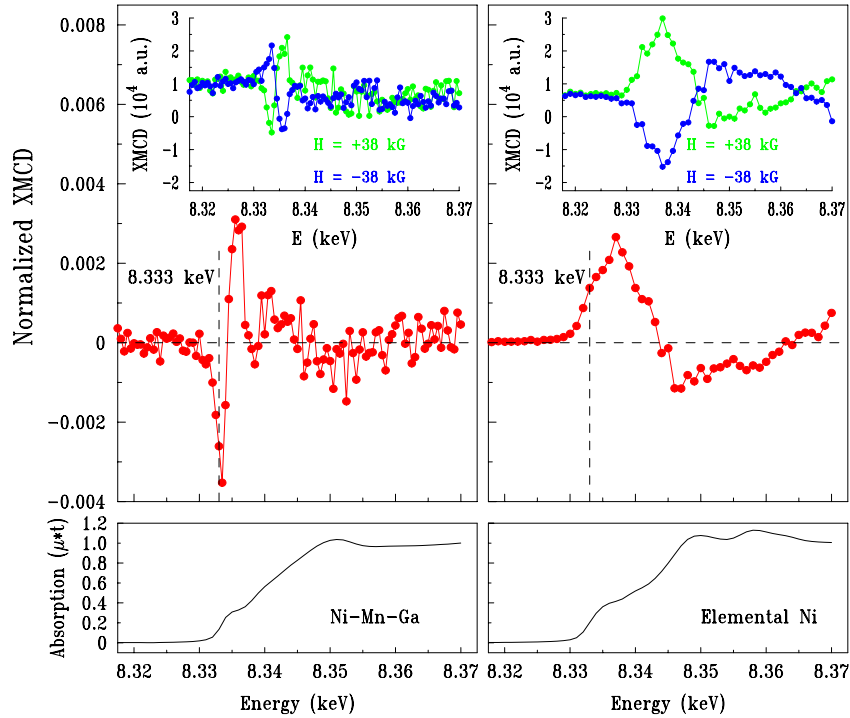


Fig. 1. Normalized XMCD spectra in Ni–Mn–Ga (left) and Ni (right). The insets show unnormalized XMCD spectra for two different field orientations with respect to the photon momentum (beam direction). The data in red were obtained by subtracting the spectra shown in the respective inset and dividing by two. The spectra were normalized to an absorption jump of one at 8.370 keV. The vertical dashed line indicates the 8.333 keV energy position. The bottom panels display the X-ray absorption profile in the respective material.

geometry with the sample oscillating $\pm 25^\circ$ in order to insure a good powder averaging.

3. Results

XMCD measures the differential absorption of circularly polarized X-rays with the helicity parallel (+) and anti-parallel (–) to the local magnetic moment through an absorption edge of an atom as a function of incident photon energy [18–20]. It is defined as

$$\text{XMCD} = \frac{1}{2}(\mu^+(E) - \mu^-(E)), \quad (1)$$

where the spin-dependent linear absorption coefficients are determined from

$$I^\pm(E) = I_0^\pm(E)e^{-\mu^\pm(E)t}, \quad (2)$$

and the total absorption coefficient is taken to be

$$\mu_0(E) = \frac{1}{2}(\mu^+(E) + \mu^-(E)). \quad (3)$$

The incident and transmitted X-ray flux for a given energy and helicity (defined above) are I_0^\pm and I^\pm and t is the thickness of the sample.

Fig. 1 displays dichroic effects at the Ni K edge observed in Ni–Mn–Ga at 4.6 K (left panels). XMCD data were also collected on a Ni foil (Fig. 1, right) as a reference. The XMCD spectra have been normalized to an absorption jump of one (bottom panels in Fig. 1). The most salient feature is that the spectra in these two materials are strikingly different. While the maximum amplitude of the

dichroism is comparable in these materials, the XMCD is spread over a wider energy range in elemental Ni than in Ni–Mn–Ga. In the latter, the primary features are confined within ± 5 eV of 8.334 keV. In both cases, XMCD reverses sign with the reversal of magnetic field direction (see insets) as it should. The XMCD data collected at several field values (not shown) showed that the maximum XMCD effect is observed above ~ 20 kG.

A spin polarization alone is known to be insufficient to produce dichroic effects at the K-edges [21–24]. SO coupling in the 4p band must be present for XMCD effects. In fact, the K-edge XMCD spectra reflect the derivative of the orbital polarization, $d\langle l_z \rangle / dE$, of the 4p states [25,26]. In addition, Guo [27] using an itinerant-electron picture relates the XMCD at the K edge to the ground-state p-projected orbital moment of the unoccupied bands [27,28]. The energy-integrated XMCD spectra up to a cutoff energy (E_c) was shown to be proportional to the orbital moment of the p states. However, the orbital-moment value was found to be dependent on E_c and the number of ‘holes’ in the p states which is difficult to know exactly in metallic systems [29,30].

Since both band-structure effects and correlations [31] between electrons, and the interaction of the excited electron with the core-hole can strongly affect XMCD [32,33], it is difficult to extract a value of the Ni 3d moment directly from the measurements. In order to obtain a value for the Ni moment and explain the qualitative differences between the two spectra, we have performed full-potential

linearized augmented plane wave (FP-LAPW) calculations [34]. Both exchange and correlation effects were taken into account as parameterized by Perdew and Wang [35]. We used the stoichiometric composition (2:1:1) for the Ni–Mn–Ga compound. 297 (68) plane waves ($RK_{\max} = 8.5(8.9)$) were used as basis functions for Ni_2MnGa (Ni); 405 k points were chosen for self-consistent calculations for both materials. For the XMCD calculations, 1470 (3349) k-points were sorted in the irreducible section of the Brillouin zone for Ni_2MnGa (Ni). The calculations have been performed for cubic structures. Note that experimentally there are no significant differences in XMCD in the martensitic and austenitic phases (see further below).

Fig. 2 shows calculated K-edge XMCD spectra for Ni_2MnGa and Ni. They have the same trends as do the experimental results. While the spectrum of pure Ni has a positive peak near the edge, the spectrum of Ni_2MnGa starts with a negative dip and grows into a positive peak. The calculated total magnetic moment of the Ni site is given by 0.328 and $0.628 \mu_B$ for Ni_2MnGa and Ni, respectively. The d-state and p-state contributions are 0.344 (0.650) and -0.008 (-0.018) μ_B , respectively, for Ni_2MnGa (Ni).

The lineshape of the XMCD spectrum in Ni_2MnGa can be explained when compared to the Ni spectrum. Their qualitative differences are due to the position of E_F in their respective density of states (DOS). Fig. 3 shows calculated XMCD in both materials with the E_F shifted to different values. For elemental Ni, we chose three energy locations for E_F , which are lower than the actual calculated E_F . For Ni_2MnGa , we employed a similar procedure as with the pure Ni but higher energies were chosen. As the E_F is lowered, the negative dip appears in pure Ni spectra (Fig. 3, right panel). In the case of Ni_2MnGa , however, the negative dip disappears and a peak similar to that in Ni spectra emerges with higher E_F (Fig. 3, left panel). Although the agreement with experimental data may not be perfect, especially at higher energies in Ni, the calculated

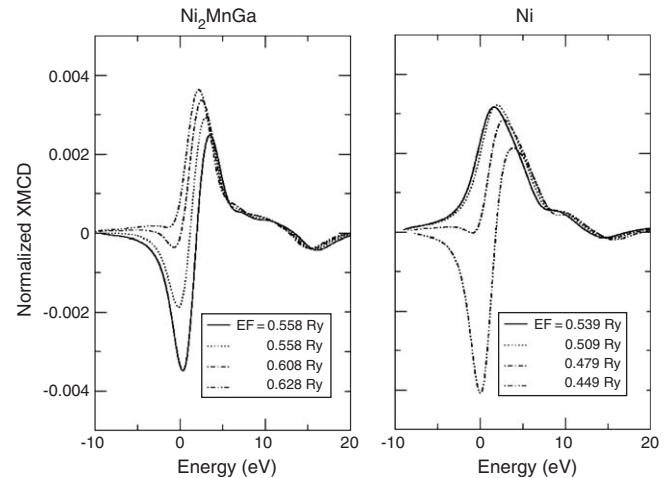


Fig. 3. XMCD spectra calculated for different values of Fermi energy in Ni_2MnGa (left) and in Ni (right).

spectra in both materials capture the essential qualitative and quantitative differences remarkably well, given that core-hole effects have been neglected.

The top panels in Fig. 4 compare the XMCD observed in the martensitic and austenitic phases at 10 and 330 K, respectively. Powder diffraction (discussed below) was performed to confirm that the material is in the austenitic phase above ~ 320 K. Except for a slight weakening of the primary features of XMCD at 330 K due to the proximity to T_c , the dichroic spectra are qualitatively similar. These observations suggest that the Ni 4p bands at and above the Fermi level are not perturbed dramatically as the material undergoes MT within the ferromagnetic phase. According to a recent study a $\sim 50\%$ increase of the Ni moment occurs in the martensitic phase [8]. It is unclear why such a large change in Ni-moment value did not leave any observable qualitative and quantitative changes in XMCD spectra. It is possible that the moment redistribution is smaller than experimentally deduced value [8], as suggested in Ref. [9]. Another possibility is the presence of an orthorhombic martensitic phase at the composition studied in this work as discussed below. A comparable decrease in Ni moment in this phase can mitigate the increase in the tetragonal phase as far as changes in the XMCD spectra is concerned.

The bottom panel (Fig. 4) shows the temperature dependence of structural powder-diffraction peaks characteristic of austenitic and martensitic phases, respectively. While the austenite phase can be indexed to the cubic structure, the low-temperature martensite contains a mixture of tetragonal and orthorhombic structures (see the insets). Although there are overlaps of multiple peaks causing significant broadening, the integrated intensities of the tetragonal $(224)_T$ and orthorhombic $(124)_O$ peaks, respectively, can be extracted by profile fitting as a function of temperature. These peaks disappear above ~ 320 K, while a sharp peak, $(422)_C$, characteristic of the cubic austenite phase grows strongly. The temperature at which MT is finished is slightly below the austenite finish (A_f)

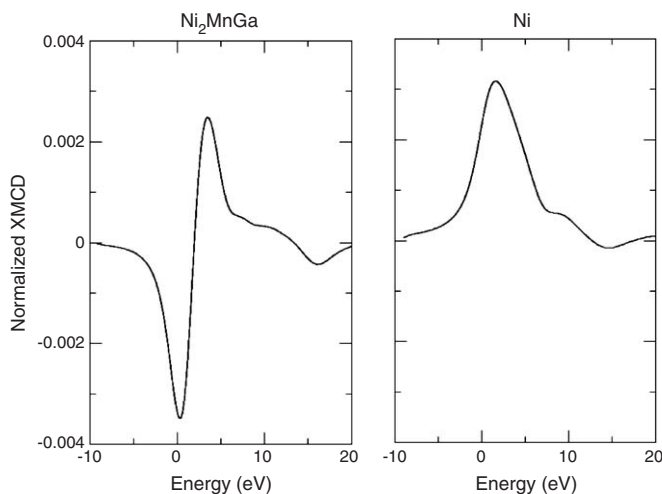


Fig. 2. Calculated XMCD spectra for Ni_2MnGa (left) and Ni (right).

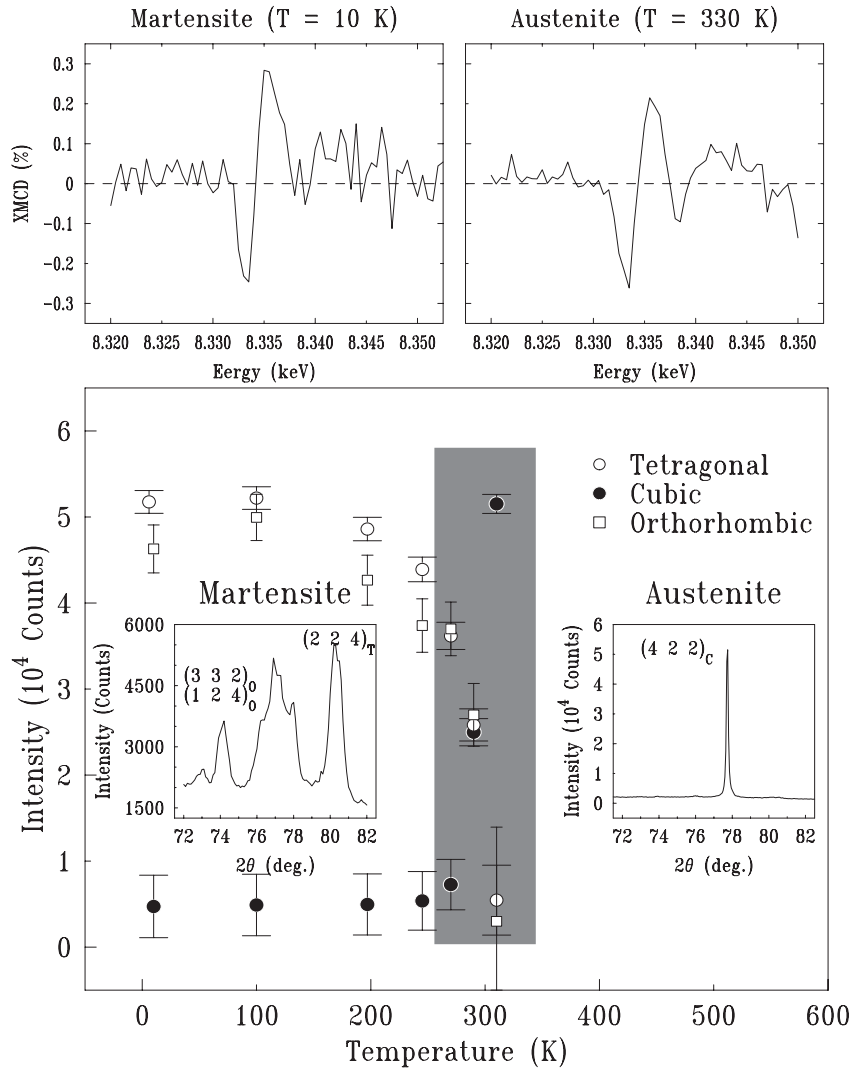


Fig. 4. XMCD (top) and MT (bottom) in Ni–Mn–Ga. The insets show sections of powder patterns in the austenite and martensite phases. Intensities of three peaks as a function of temperature are displayed using different symbols. Data were collected on warming. The shaded area depicts the approximate transformation range in temperature.

temperature (Table 1). This reduction may be related to resin-induced stress on the particulates that are subject to varying temperatures, which can affect structural properties [36]. We note that, for the composition studied in this work the coexistence of two martensitic phases has been reported earlier [37]. We speculate that the feature at ~ 280 K in the DSC measurements is related to a MT from the orthorhombic martensite, which has a slightly lower transition temperature than does the tetragonal martensite. Measurements on single crystals are necessary to confirm this hypothesis.

4. Summary

In summary, we provided unambiguous, model-independent, and element-specific experimental evidence for the existence of significant 3d moment at the Ni site in Ni–Mn–Ga FSMA. By comparative experimental and band theoretical studies of XMCD spectra in Ni–Mn–Ga

and elemental Ni we deduced the value of Ni moment in Ni–Mn–Ga to be $\sim 0.33 \mu_B$. Furthermore, striking differences between the XMCD spectra in these two materials have been explained by relative shifts of the Fermi level with respect to the electronic DOS in these materials. Theoretical studies of magnetic excitations [5] and interplay of ferromagnetism and MT in these materials must take into account the presence of significant Ni moments in Ni–Mn–Ga alloys.

Acknowledgements

We thank W. E. Straszheim (ISU) for determining the chemical composition of the Ni–Mn–Ga alloy studied in this work. The Advanced Photon Source is supported by the DOE (Basic Energy Sciences), Contract No. W-31-109-ENG-38. Ames Laboratory is operated by Iowa State University under USDOE Contract No. W-7405-Eng-82.

References

- [1] F. Heusler, *Z. Angew. Chem.* 17 (1904) 260.
- [2] K. Ullakko, J.K. Huang, C. Kantner, V.V. Kokorin, R.C. O'Handley, *Appl. Phys. Lett.* 69 (1996) 13.
- [3] S.J. Murray, M.A. Marioni, A.M. Kukla, J. Robinson, R.C. O'Handley, S.M. Allen, *J. Appl. Phys.* 87 (2000) 5774.
- [4] P.J. Webster, K.R.A. Ziebeck, S.L. Town, M.S. Peak, *Philos. Mag.* B 49 (1984) 295.
- [5] J. Enkovaara, A. Ayuela, J. Jalkanen, L. Nordström, R.M. Nieminen, *Phys. Rev. B* 67 (2003) 054417.
- [6] M. Pajda, J. Kudrnovský, I. Turek, V. Drchal, P. Bruno, *Phys. Rev. B* 64 (2001) 174402.
- [7] J. Kübler, A.R. Williams, C.B. Sommers, *Phys. Rev. B* 28 (1983) 1745.
- [8] P.J. Brown, A.Y. Bargawi, J. Crangles, K.-U. Neumann, K.R.A. Ziebeck, *J. Phys.: Condens. Matter* 11 (1999) 4715.
- [9] S. Fuji, S. Ishida, S. Asano, *J. Phys. Soc. Japan* 58 (1989) 3657.
- [10] A.N. Vasil'v, A.D. Bozhko, V.V. Khovailo, I.E. Dikhstein, V.G. Shavrov, V.D. Buchelnikov, M. Matsumoto, S. Suzuki, T. Takagi, J. Tani, *Phys. Rev. B* 59 (1999) 1113.
- [11] C. Jiang, G. Feng, S. Gong, H. Xu, *Mater. Sci. Eng. A* 342 (2003) 231.
- [12] F. Albertini, L. Pareti, A. Paoluzi, L. Morellon, P.A. Algarabel, M.R. Ibarra, L. Righi, *Appl. Phys. Lett.* 81 (2002) 4032.
- [13] Y. Lee, J.Y. Rhee, B.N. Harmon, *Phys. Rev. B* 66 (2002) 054424.
- [14] A. Zheludev, S.M. Shapiro, P. Wochner, A. Schwartz, M. Wall, L.E. Tanner, *Phys. Rev. B* 51 (1995) 11310.
- [15] U. Stuhr, P. Vorderwisch, V.V. Kokorin, P.-A. Lindgård, *Phys. Rev. B* 56 (1997) 14360.
- [16] K. Hirano, T. Ishikawa, S. Kikuta, *Nucl. Instrum. Meas. A* 336 (1993) 343.
- [17] M. Suzuki, N. Kawamura, M. Mizumaki, A. Urata, H. Maruyama, S. Goto, T. Ishikawa, *J. Appl. Phys. Japan* 37 (1998) L1488.
- [18] G. Schütz, W. Wagner, W. Wilhelm, W. Kienle, P. Zeller, R. Frahm, G. Materlik, *Phys. Rev. Lett.* 58 (1987) 737.
- [19] G. Schütz, R. Frahm, R. Wienke, W. Wilhelm, W. Kienle, *Rev. Sci. Instrum.* 60 (1989) 1661.
- [20] G. Schütz, P. Fischer, K. Attenkofer, M. Knülle, D. Ahlers, S. Stähler, C. Detlefs, H. Ebert, F.M.F. de Groot, *J. Appl. Phys.* 76 (1994) 6453.
- [21] S. Stähler, G. Schütz, H. Ebert, *Phys. Rev. B* 47 (1993) 818.
- [22] J. Stöhr, Y. Wu, in: A.S. Schlachter, F.J. Wuilleumier (Eds.), *New Directions in Research with Third-Generation Soft X-Ray Synchrotron Radiation Sources*, Kluwer Academic Publishers, Boston, 1994, p. 221.
- [23] V.N. Antonov, B.N. Harmon, A.N. Yaresko, *Phys. Rev. B* 67 (2003) 24417.
- [24] M.S.S. Brooks, B. Johansson, in: H. Ebert, G. Schütz (Eds.), *Spin-Orbit Influenced Spectroscopies*, Springer, Heidelberg, 1996, p. 211.
- [25] H.J. Gotsis, P. Strange, *J. Phys.: Condens. Matter* 6 (1994) 1409.
- [26] H. Ebert, in: H. Ebert, G. Schütz (Eds.), *Spin-Orbit Influenced Spectroscopies*, Springer, Heidelberg, 1996, p. 160.
- [27] G.Y. Guo, *J. Phys.: Condens. Matter* 8 (1996) L747.
- [28] G.Y. Guo, *Phys. Rev. B* 57 (1998) 10295.
- [29] R. Wu, D. Wang, A.J. Freeman, *Phys. Rev. Lett.* 71 (1993) 3581.
- [30] R. Wu, A.J. Freeman, *Phys. Rev. Lett.* 73 (1994) 1994.
- [31] L.H. Tjeng, C.T. Chen, P. Rudolf, G. Meigs, G. van der Laan, B.T. Thole, *Phys. Rev. B* 48 (1994) 13378.
- [32] J. Zaanen, G.A. Sawatzky, J. Fink, W. Speier, J.C. Fuggle, *Phys. Rev. B* 37 (1985) 4905.
- [33] J. Schwitalla, H. Ebert, *Phys. Rev. Lett.* 80 (1998) 4586.
- [34] P. Blaha, K. Schwarz, P. Sorantin, S.B. Trickey, *Comput. Phys. Commun.* 59 (1990) 399.
- [35] J.P. Perdew, Y. Wang, *Phys. Rev. B* 45 (1992) 13244.
- [36] V.V. Martynov, V.V. Kokorin, *J. Phys. III* 2 (1992) 739.
- [37] N. Glavatska, G. Mogiliniy, I. Glavatska, S. Danikin, D. Hohlwein, A. Beskrovnij, O. Söderberg, V.K. Lindroos, *J. Phys. IV* 112 (2003) 963.